The Three-Dimensional Structure of Water Confined in Nanoporous Vycor Glass

ARTICLE *in* THE JOURNAL OF PHYSICAL CHEMISTRY B · JUNE 2007

Impact Factor: 3.3 · DOI: 10.1021/jp0677905 · Source: PubMed

The Three-Dimensional Structure of Water Confined in Nanoporous Vycor Glass

Helen Thompson,[†] Alan K. Soper,[*,†] Maria Antonietta Ricci,[‡] Fabio Bruni,[‡] and Neal T. Skipper[§]

ISIS Facility, Rutherford Appleton Laboratory, Didcot, OXON, OX11 0QX, United Kingdom, Dipartimento di Fisica, Università Roma Tre Via della vasca navale 84, I-00146 Rome, Italy, and Department of Physics and Astronomy, University College London, Gower Street, London WC1E 6BT, United Kingdom

Received: November 23, 2006; In Final Form: March 28, 2007

Neutron diffraction data, in conjunction with isotopic substitution of deuterium (D) for hydrogen (H), have been analyzed to determine the three-dimensional structure of water confined in vycor, an archetypal hydrophilic porous silica glass containing channels or pores of ∼40 Å diameter. The data have been incorporated into a Monte Carlo computer simulation of the confined water system, and the site−site potentials have been iteratively refined in order to produce a model ensemble which is consistent with both the neutron diffraction data and two possible geometries of the vycor pores (cylindrical and spherical). This approach has allowed us to investigate in detail the contributions to the experimentally accessible partial pair correlation functions, and ascertain whether particular features arise from interactions of the water molecules with the substrate surface, or from purely geometrical confinement effects. We observe a significant decrease in the first shell water oxygen−oxygen co-ordination number, and a decrease in the number of hydrogen bonds per water molecule from ∼3.6 in bulk water to ∼2.2 in confinement. In addition, we observe a significant shift inward of the second peak in the water oxygen−water oxygen coordination shell. Overall, we therefore find that the structure of the water in vycor is strongly perturbed relative to the bulk.

1. Introduction

Water is ubiquitous as a solvent in the physical and biological sciences, and plays a central role in an extraordinary number of natural and industrial processes, for example, protein folding, enzymatic activity, membrane stability, molecular filtration, mineral diagenesis, oil recovery, and hydrate formation. In these and many other important situations, the water is not always present in its bulk form, but is often confined within mesoporous or interfacial environments. Understanding and controlling the microscopic and thermodynamic properties of confined water is currently a major research challenge, with many key questions centering on the nature and extent of molecular-scale restructuring in the liquid.[1−4] In this context, particular attention is focused on the response of the hydrogen-bonding network to confinement.[1,2]

Confined water has been the subject of numerous diffraction experiments.[1,2,5,6] These draw sometimes conflicting conclusions based on the difference between the data for the confined liquid and the liquid in the bulk. For example, neutron diffraction studies of D_2O in hydrophilic confinement have pointed to a thin layer of surface water with a greater extent of hydrogen bonding and lower density than bulk water.[7,8,9] However, experiments exploiting isotopic labeling have pointed to a reduction in hydrogen bonds and lower tetrahedral order.[5,10] In the case of confined fluids, after subtraction of the dry substrate diffraction pattern, it has been shown that the weightings of the fluid-substrate terms are not insignificant,[5] and in the case of deuterated water confined in vycor, these terms are calculated to contribute up to 73% in the total structure factors (see Table 1). For this reason it is difficult to distinguish water−water correlations from water−substrate correlations via experimental data alone. Hence it is impossible to know whether the differences in the partial pair correlation functions between bulk and confined water are due to true changes in the water structure upon confinement, or to these additional water−substrate cross correlation terms,[5] without recourse to some form of molecular modeling.

TABLE 1: Relative Weights of Each Pair−Pair Correlation for the Confined Water Total Structure Factors in the Spherical Pore Simulation

	weighting factor		
	D_2O	H_2O	HDO
Si−OW	0.0116	0.0116	0.0116
Si−HW	0.0265	−0.0149	0.0100
nbO−OW	0.0027	0.0027	0.0027
nbO−HW	0.0061	−0.0034	0.0023
H−OW	0.0031	−0.0017	0.0012
H−HW	0.0071	0.0022	0.0010
bO−OW	0.0318	0.0318	0.0318
bO−HW	0.0732	−0.0410	0.0275
OW−OW	0.0056	0.0056	0.0056
OW−HW	0.0259	−0.0145	0.0097
HW−HW	0.0298	0.0094	0.0042

The difficulty in coming to a full understanding of the structure of confined water via purely experimental data highlights the need for a fully integrated approach exploiting complementary atomistic-level simulation of the system. This would enable us to extract the partial pair correlation functions relating to the confined water minus the water−substrate terms, providing accurate structural data for quantitative comparison with the bulk liquid. Previous simulations of fluids in confined geometries have attempted to address these issues[3,11,12,13] and have been compared with similar simulations of bulk liquids,

* Corresponding author. E-mail: a.k.soper@rl.ac.uk.
† Rutherford Appleton Laboratory.
‡ Universita' di Roma Tre Via della Vasca Navale 84.
§ University College London.

10.1021/jp0677905 CCC: $37.00
Published on Web 05/02/2007

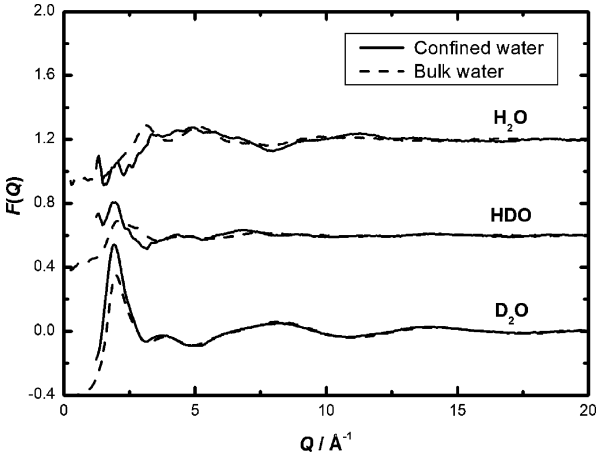

Figure 1. A comparison of the confined water total structure factors: D_2O, HDO, and H_2O, with those from bulk water, showing significant differences in the intermolecular structure below 5 $Å^{-1}$.

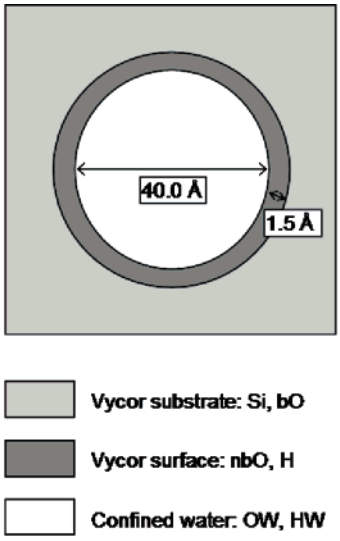

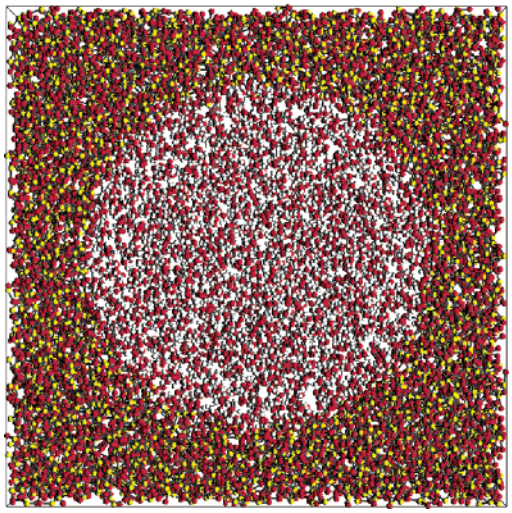

Figure 2. A cross section of the simulation cell, showing the excluded volume regions for each atom type, and a molecular snapshot of the simulation cell for the cylindrical pore. The uniform atom distributions have been calculated from a random distribution of points in each of these regions.

but at no stage has any direct comparison been made between simulation and experimental data. This is due to the topological differences between the simulation cell and the real sample, and

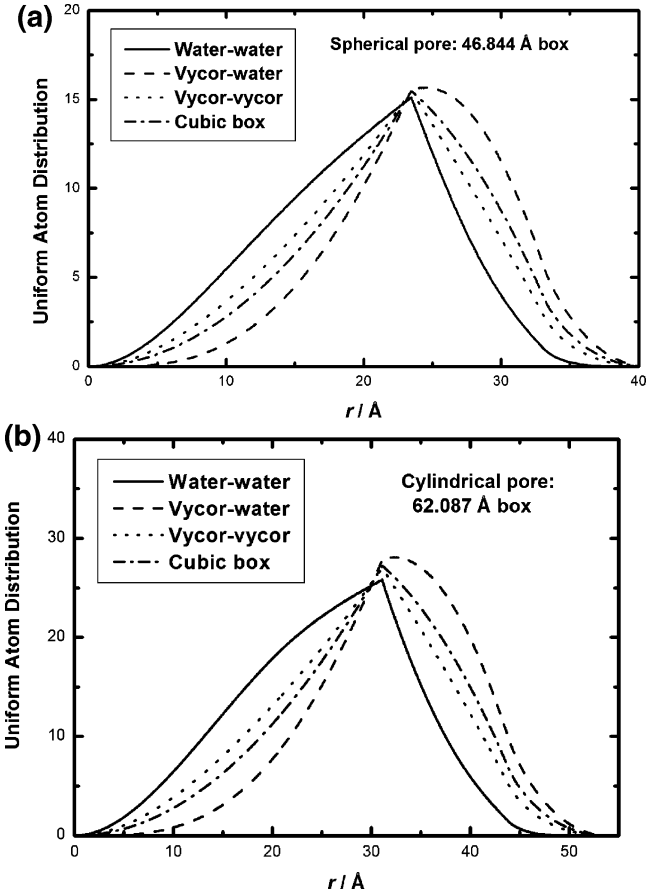

Figure 3. The uniform atom distributions for water−water, vycor−water, vycor−vycor correlations, as compared to a homogeneous bulk liquid in a cubic box: (a) spherical pore, (b) cylindrical pore. Note the steeper initial rise for the confined water $n(r)$ than for bulk water in a cubic box.

TABLE 2: The Lennard−Jones Potential Parameters and Charges Used for the Vycor Substrate and Confined Water Atoms

	potential parameters		
	σ (Å)	ϵ (kJ/mol)	q (e)
Si	0.760	0.80	+3.0
nbO	3.560	0.65	−1.0
H	0.000	0.00	+1.0
bO	3.560	0.65	−1.5
OW	3.166	0.65	−0.8476
HW	0.000	0.00	0.4238

the fact that the water molecule potentials used in those simulations would not reproduce the experimental site−site distribution functions for bulk water.

In order to resolve these issues, it is first necessary to use a relatively simple and well-characterized substrate. In this paper we have chosen to study a well characterized vycor glass, which contains a random network of pores of diameter 40 ± 5 Å.[2] The structure of vycor is similar to bulk silica glass, with silicon atoms 4-fold coordinated to oxygen atoms. The surface of the pore is hydrophilic, consisting of acidic OH groups. As a result, water interacts strongly with the substrate surface, and both the thermodynamics and molecular motions are significantly different from those in the bulk.[4,14,15] Specifically, there is a decrease in enthalpy and entropy[14] and an overall slowing of the dynamics[4,15−17] on confinement. Moreover, freezing is found to be incomplete even at 240 K,[14] and the critical point is depressed in both temperature and pressure.[18] The challenge

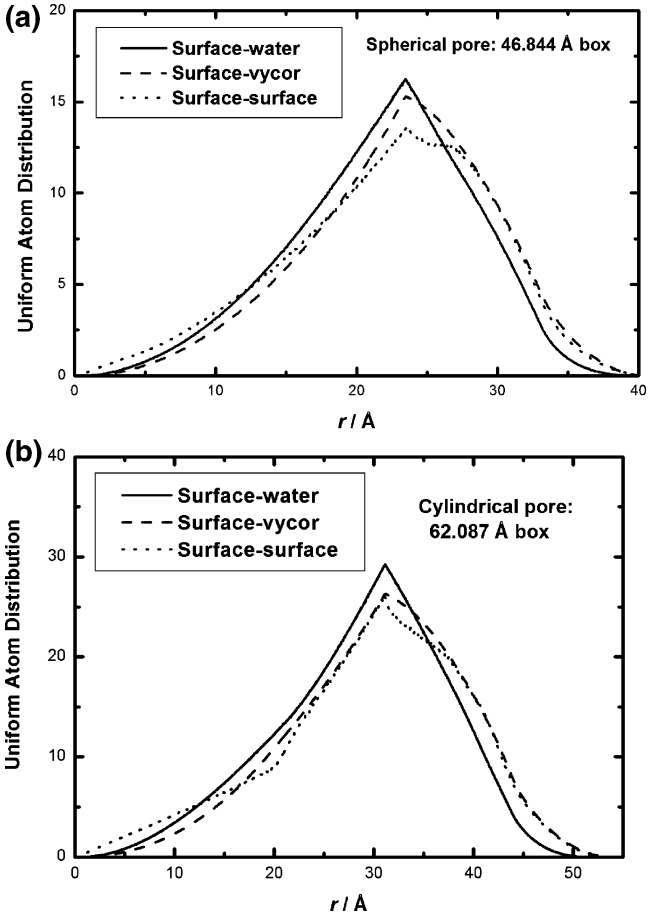

Figure 4. The uniform atom distributions for surface water, surface−vycor, and surface−surface correlations: (a) spherical pore, (b) cylindrical pore.

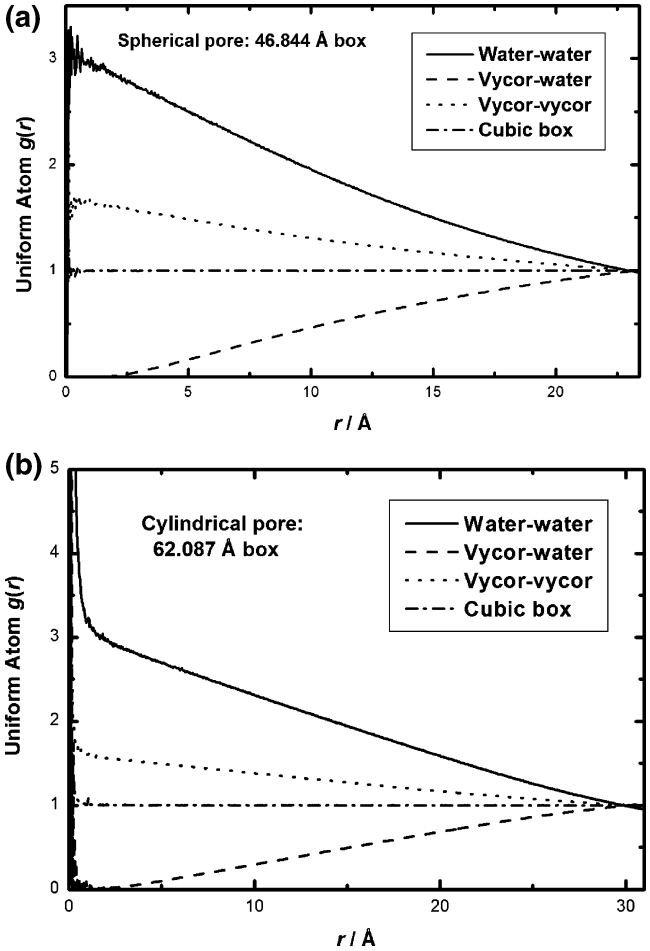

Figure 5. The corresponding pair distribution function for water−water, vycor−water, and vycor−vycor correlations, as compared to a homogeneous bulk liquid in a cubic box: (a) spherical pore, (b) cylindrical pore, calculated using eq 4. The downward slope for water−water and vycor−vycor uniform atom $g(r)$s arises because the local water/vycor density "seen" by a water/vycor molecule is higher than the bulk water/vycor density. The upward slope for the water−vycor uniform atom $g(r)$ is because the local vycor density 'seen' by a water molecule is lower than the average vycor density.

we now address is to relate these observations to the microscopic structure of the confined water.

In this paper we use the technique of empirical potential structure refinement (EPSR)[19,20,21] to simulate water confined in a pore of ∼20 Å radius, first performing a standard Monte Carlo simulation of the system and comparing the structure with the neutron diffraction data, and second using the neutron diffraction data to drive the simulation such that the resulting configuration is consistent with the measured data. We show that confinement of water introduces significant changes in the first and second hydration shells as seen in the OW−OW distribution function, and we observe differences in the OW−HW and HW−HW distribution functions in the region around 2−3 Å where the main signatures of hydrogen-bonding occur.

2. Experimental Method

Neutron diffraction data have been collected for three samples of dry vycor,[5] the nonbridging oxygen atoms having been saturated with hydrogen, deuterium, and a 40:60 mixture of hydrogen and deuterium. It should be noted that in the original publication of this data,[5] the experimental value of a 50:50 mixture of hydrogen and deuterium was reported—it was only upon modeling the data in the present work that we found a 40:60 mixture gave a closer fit to the data. In addition, data were collected for vycor fully hydrated (i.e., pores filled) with H_2O, D_2O and a 40:60 mixture of H_2O and D_2O. The volume fraction of the pores was 0.326, and the water had a lower density than bulk water of 0.0891 atoms Å^{-3}, as compared to 0.1 atoms Å^{-3} for bulk water.

Data analysis was carried out using the Gudrun package, a new implementation of the ATLAS routines.[22] The dry vycor data were corrected for absorption, multiple scattering, backgrounds (empty cell and instrument) and self-scattering, and normalized per atom. For the fully hydrated samples, the "sample" was defined as the confined water alone, and the dry vycor plus the titanium−zirconium null coherent scattering cell was given as the "container". After the corrections for multiple scattering, absorption, and background and dry vycor plus cell subtraction, we obtain three differential cross-section datasets, for confined D_2O, H_2O and HDO. The self-scattering contribution was then subtracted from these datasets, using a semiempirical method of subtracting a low-order polynomial from the DCS as outlined in ref 23, yielding the total structure factors $F(Q)$ for confined D_2O, H_2O and HDO.

The total structure factor obtained from each diffraction experiment is a sum of all the individual partial structure factors, i.e., all water−water, water−substrate, and substrate−substrate terms, given by

$$F(Q) = \sum c_\alpha c_\beta b_\alpha b_\beta S_{\alpha\beta}(Q) \qquad (1)$$

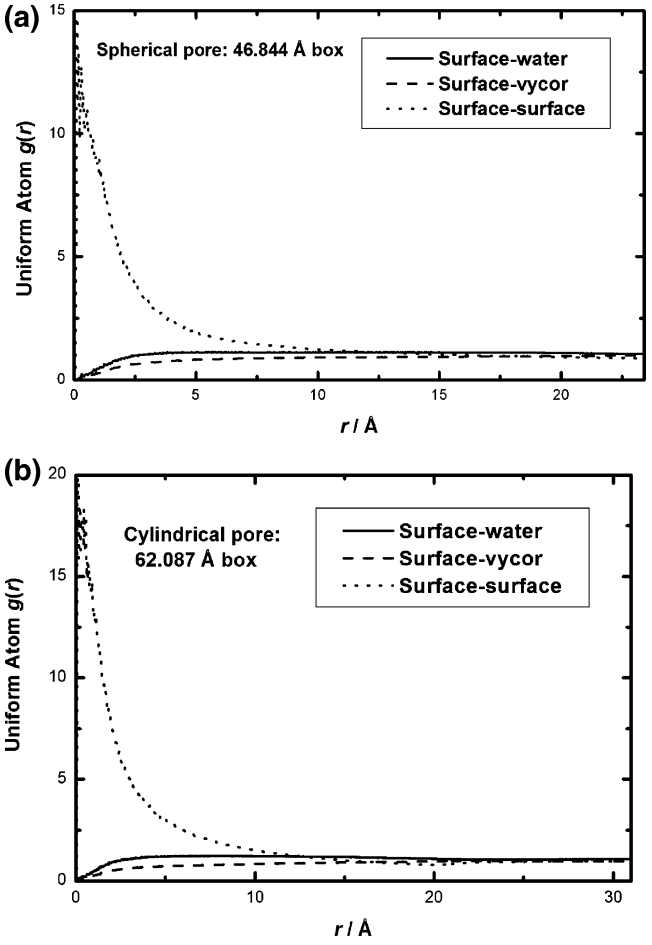

Figure 6. The corresponding pair distribution function for surface water, surface−vycor, and surface−surface correlations: (a) spherical pore, (b) cylindrical pore, calculated using eq 4.

The partial structure factor is related to the partial pair correlation function (g(r)) via a Fourier transform:

$$g_{\alpha\beta}(r) - 1 = \frac{1}{2\pi^2\rho_0 r}\int_0^\infty Q[S_{\alpha\beta}(Q) - 1]\sin(Qr)\,dQ \quad (2)$$

The radial distribution function G(r) is given by

$$G_{\alpha\beta}(r) = 4\pi\rho_0 r^2 g_{\alpha\beta}(r) \quad (3)$$

The resulting total structure factors are shown in Figure 1, and are compared with bulk water data, and the relative weights for each atom pair are given in Table 1.

In order to be able to compare the structure of confined water with bulk water and to determine the effects of the hydrophilic surface on the water structure, it is necessary to separate these terms into individual partial structure factors. To tackle this problem we turn to the EPSR[19−21] computer simulation of the system, in which the interatomic potentials are empirically refined in order to model the neutron diffraction data.

3. Computer Simulation Analysis

3.1. The Simulation Cells. The initial requirement for simulating water confined in vycor glass is to construct a realistic model of the dry vycor substrate, and the starting point for this is to create a model of bulk silica. The structure factor for bulk silica was measured in a separate experiment using a silica slab with a thickness of ∼2 mm. A simulation of bulk silica in a 46.8466 Å box was then performed using the EPSR program, with the charges and reference potentials as given in Table 2. The values for σ and ϵ were chosen to give the best initial fit to the bulk silica diffraction data. These starting potentials were then refined against the total structure factor for bulk silica. The simulation was not refined against the dry vycor data at this stage. When the fit to the data was satisfactory, the simulation cell was modified to create a single spherical pore of radius ∼20.0 Å, as follows:

(a) A cavity was created inside the silica, by removing all atoms which lay within $r = 20.0$ Å from the center, i.e., those for which the coordinates $x^2 + y^2 + z^2 < 20.0^2$. (Note that in vycor glass, the pores are randomly arranged and have a narrow distribution of radii, the average pore radius being 20 Å. The initial box size of 46.8466 Å was used here so that the void fraction of the simulated vycor cell would be equal to the experimental value of 0.326).

(b) Next, the coordination number of oxygen atoms around each silicon atom within 1.5 Å of the pore surface was calculated. Any silicon atoms with an oxygen co-ordination number of less than 4 were removed.

(c) Next, the co-ordination number of silicon atoms around each oxygen atom within 1.5 Å of the pore surface was calculated. If the silicon coordination number around any these surface oxygen atoms was found to be greater than or equal to 2, the oxygen atom was termed a "bridging oxygen" (bO). If the silicon co-ordination number for the surface oxygen atom was 1, the atom was termed a "nonbridging oxygen" (nbO), and a hydrogen atom was then included to saturate the oxygen, at an equilibrium distance of 0.95 Å, at an angle such that the O−H bond was directed toward the center of the pore. If the silicon co-ordination number of each surface oxygen atom was found to be zero, the oxygen atom was removed from the system.

(d) The EPSR simulation was then run on the vycor substrate alone for several iterations, in order to relax the angles of the O−H groups and create a rough pore surface. The structure factor obtained from the simulation at this stage provided a acceptable fit to the experimentally determined structure factors for the dry vycor, in the sense that the simulated structure was able to reproduce all the main peak positions and heights in the data, with only minor discrepancies remaining.

Having created a realistic simulation cell for the dry vycor, 995 water molecules were introduced into the simulation cell at a density of 0.0891 atoms Å^{-3}, and assigned random positions within the spherical pore. The water reference potentials were those for SPC/E water,[24] and the O−H and H−H average intramolecular distances were set as 0.976 and 1.55 Å, respectively (i.e., the distances obtained via experimental data on bulk water).

A separate simulation cell was created to model the water confined within a cylindrical pore, in order to confirm that any changes in the water structure were not simply a function of the pore geometry. A simulation of bulk silica was performed in a 62.0870 Å box, and a cylindrical pore of radius 20.0 Å was created by removing all atoms which lay within this pore (i.e., those for which the coordinates $x^2 + y^2 < 20.0^2$). The box size was chosen to ensure that the void fraction here again matched the experimental value. As described above, the coordination numbers of the silicon and oxygen atoms were checked in the same way, and any nonbridging oxygens were saturated with a hydrogen atom. After running a few iterations on the vycor substrate alone, 2317 water molecules were introduced into the cylindrical pore with random coordinates, again at the experimental density of 0.0891 atoms Å^{-3}.

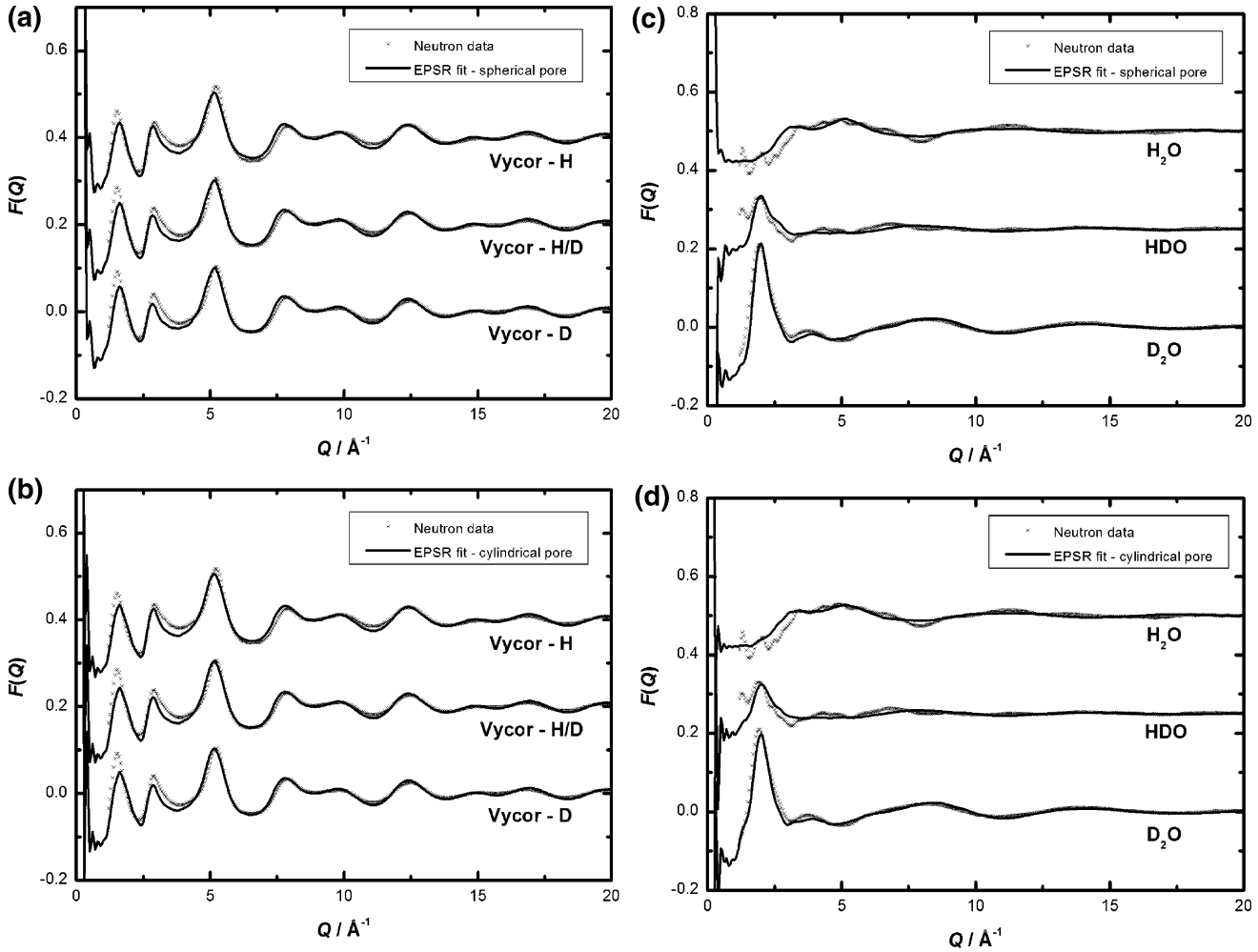

Figure 7. The EPSR fits to the neutron total structure factors for the dry vycor samples: (a) spherical pore, (b) cylindrical pore, and the EPSR fits to the total structure factors for the confined water, obtained from the fully hydrated vycor data: (c) spherical pore, (d) cylindrical pore. Note that the data and fit have been scaled by factors of (number of vycor atoms/total number of atoms) and (number of water atoms/total number of atoms) respectively.

3.2. The Uniform Atom Distribution. When water is confined in a porous network, the molecular structure as seen in the pair correlation functions is affected by its geometrical confinement, as well as interactions with the substrate. This dependence on the allowed positions of particular molecule types is known as the "excluded volume effect" and must be taken account of if any comparison is to be made between the structure of confined water and bulk water.[10,25]

For a cubic box, the uniform atom distribution increases as r approaches the edge of the box, then decreases rapidly to zero as r tends to the corners of the box, and can be calculated analytically. However, this calculation is not straightforward if the box contains heterogeneities, as is the case here. The uniform atom distributions used in the simulations were calculated by assigning random positions to 5000 atoms within a cubic box. The water−water (WW) uniform atom distribution was calculated by considering only those atoms which lay within the pore, i.e., those for which $\sqrt{x^2+y^2+z^2} < 20.0$ Å for the spherical pore, or $\sqrt{x^2+y^2} < 20.0$ Å for the cylindrical pore, and creating a histogram of the distances between each atom pair. The minimum image convention was used in this calculation. Similarly for the substrate−water uniform atom distribution, the pairs of atoms counted were those for which one atom lay outside the pore and one atom lay within the pore, and for the substrate−substrate uniform atom calculation, the pairs included were solely those for which both atoms lay outside the pore. The distributions were then normalized to the total number of atoms used in the EPSR simulation, by multiplying the number of atoms counted within each histogram bin of 0.03 Å by the total number of atoms in the EPSR simulation cell, and dividing by the number of pairs of atoms counted for each uniform atom distribution.

Within the simulation cell, it has already been noted that the surface nonbridging oxygen atoms are labeled as a different species, "nbO", compared to the bridging oxygens within the substrate, labeled "bO". So unlike the experimental analysis which considers only two volume regions (water and vycor substrate) it is now necessary to define three regions: the water-filled sphere (W), the pore surface (S), which is defined as an annulus of 1.5 Å around the pore, and the region within the vycor substrate (V), as shown in Figure 2. In total, 6 sets of uniform atom distributions were calculated: vycor−vycor, vycor-surface, vycor−water, water−water, water−surface and surface−surface. The atom types included as 'vycor' were then Si and bO, those as "water" were OW and HW, and those as "surface" were nbO and H. The equivalent uniform atom partial pair correlation functions were calculated in the standard way, using

$$g^{\mathrm{uni}}(r) = \frac{n(r)V}{(\text{number of pairs})4\pi r^2 \Delta r} \qquad (4)$$

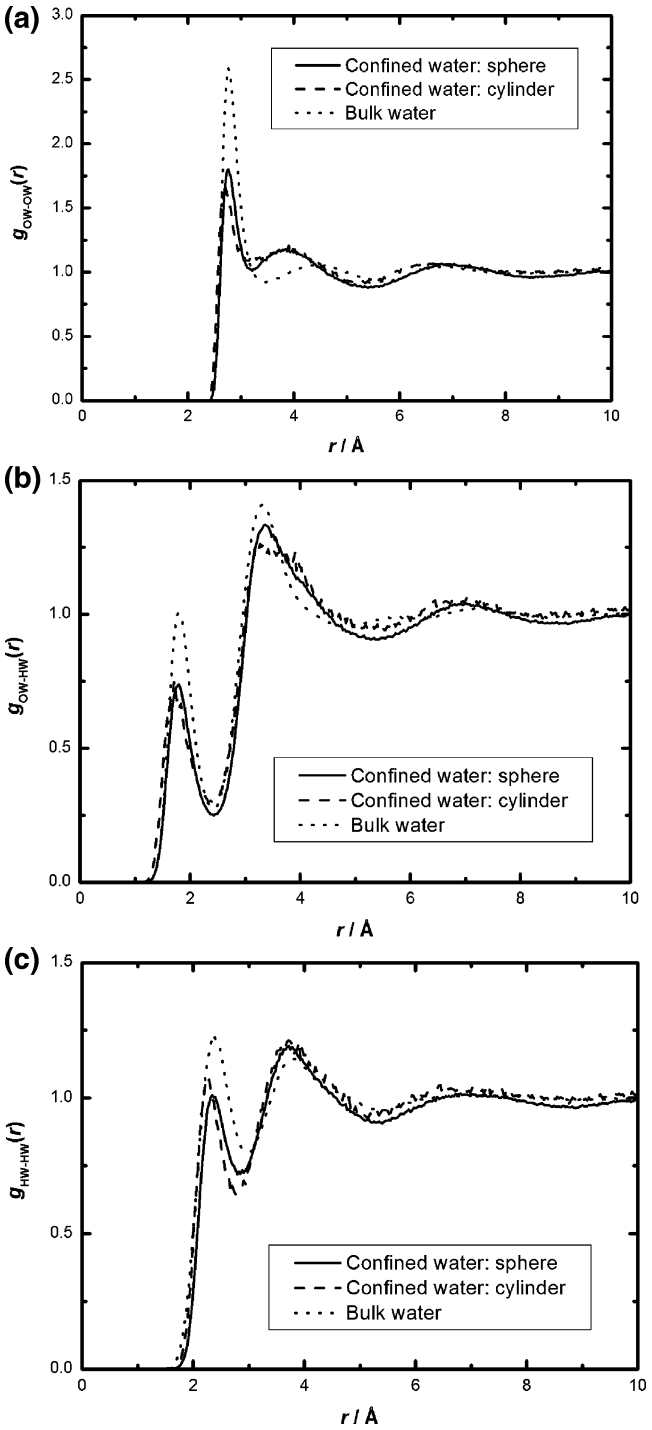

Figure 8. The partial pair correlation functions for confined water: comparison between water confined in a spherical pore, water confined in a cylindrical pore, and bulk water: (a) oxygen−oxygen, (b) oxygen−hydrogen, (c) hydrogen−hydrogen.

This calculation was performed using 5000 random coordinates, and was repeated every ten iterations during the EPSR simulation, to minimize any statistical noise arising from this method of correction for the excluded volume effect. The uniform atom distributions, $n(r)$, and equivalent radial distribution functions are shown in Figures 3−6 for both the geometries investigated. We notice both quantitative and qualitative differences in the functions calculated for the spherical pore and the cylindrical pore, with the most significant difference appearing in the water−water distribution.

The EPSR simulation program was then modified such that each atom−atom $n(r)$ derived from the simulation was divided by the appropriate uniform atom distribution. In addition, the partial pair correlation functions extracted from the Q-space data via a direct Fourier transform were divided by the appropriate uniform atom $g(r)$ calculated as described above. In the simulations for both the spherical pore and cylindrical pore, using a pore radius of 20.0 Å in the uniform atom calculation gave rise to a slope with positive gradient underlying the partial pair correlation functions, showing that the uniform atom distribution was not fully accounting for the excluded volume effect. Trial and error showed that using a slightly larger pore radius of 20.2 Å in the uniform atom calculation was more accurate: this slightly larger value is perhaps a consequence of the method in which the pore was created within the simulation cell, or maybe results from the roughness of the pore surface as the nonbridging oxygen atoms are saturated with hydrogen atoms. Using this method of "tuning" the pore radius, the real-space functions arising from both simulation and experiment were ensured to remain on a level and oscillate around 1.0 at higher r.

3.3. Incorporating the Experimental Data. The relative weighting factors of the pair correlations for each dataset were calculated initially in the normal way, using the product of the scattering lengths and atomic fractions (as calculated from the whole simulation cell of both water and vycor) for the atom types.

Then for the water only diffraction datasets, any contributions from the substrate−substrate correlations were set to zero, since the data contain only water−water and water−substrate correlations. Similarly, for the dry vycor datasets, any contributions from water−water or water−vycor terms were set to zero, since these data only contain vycor−vycor correlations.

This method of weights calculation uses the atomic fractions as calculated from the whole of the simulation cell, whereas the data have been scaled either to the number of water atoms or the number of vycor atoms. In order to incorporate the data into the simulation, the water data must be rescaled to the total number of atoms in the simulation cell (i.e., multiplied by the number of water atoms and divided by the total number of atoms). In addition, the vycor data must also be rescaled to the total number of atoms in the cell (i.e., multiplied by the number of vycor atoms and divided by the total number of atoms).

3.4. Running the EPSR Simulation. At the start of the simulation of the confined water−vycor system, the substrate atoms and surface hydrogens were held fixed in position, the coordinates of the H atoms having already been relaxed by running a simulation of the substrate alone for several iterations, creating a rough pore surface. The potential parameters and charges for the silica Si, bO, nbO, and H atoms, and the water OW and HW are given in Table 2. The Monte Carlo simulation was run with moves allowed for water molecules only until the cell had equilibrated. This was done to prevent the randomly arranged water molecules inducing too large a change in the initial vycor structure. The simulations required ∼75 equilibration steps for the spherical pore and ∼175 steps for the cylindrical pore.

Next, the simulation was performed as a standard Monte Carlo with moves allowed for both the confined water and the vycor substrate molecules, but with no dependence on the diffraction data. A confidence factor of 0.95 was then applied to the data, and an inversion matrix method[26] was used to create the individual partial structure factors. From this stage, a perturbation to the initial reference potential can be calculated from the difference between the fit and the data for each pair of atom types, as in the standard EPSR algorithm. The potential used

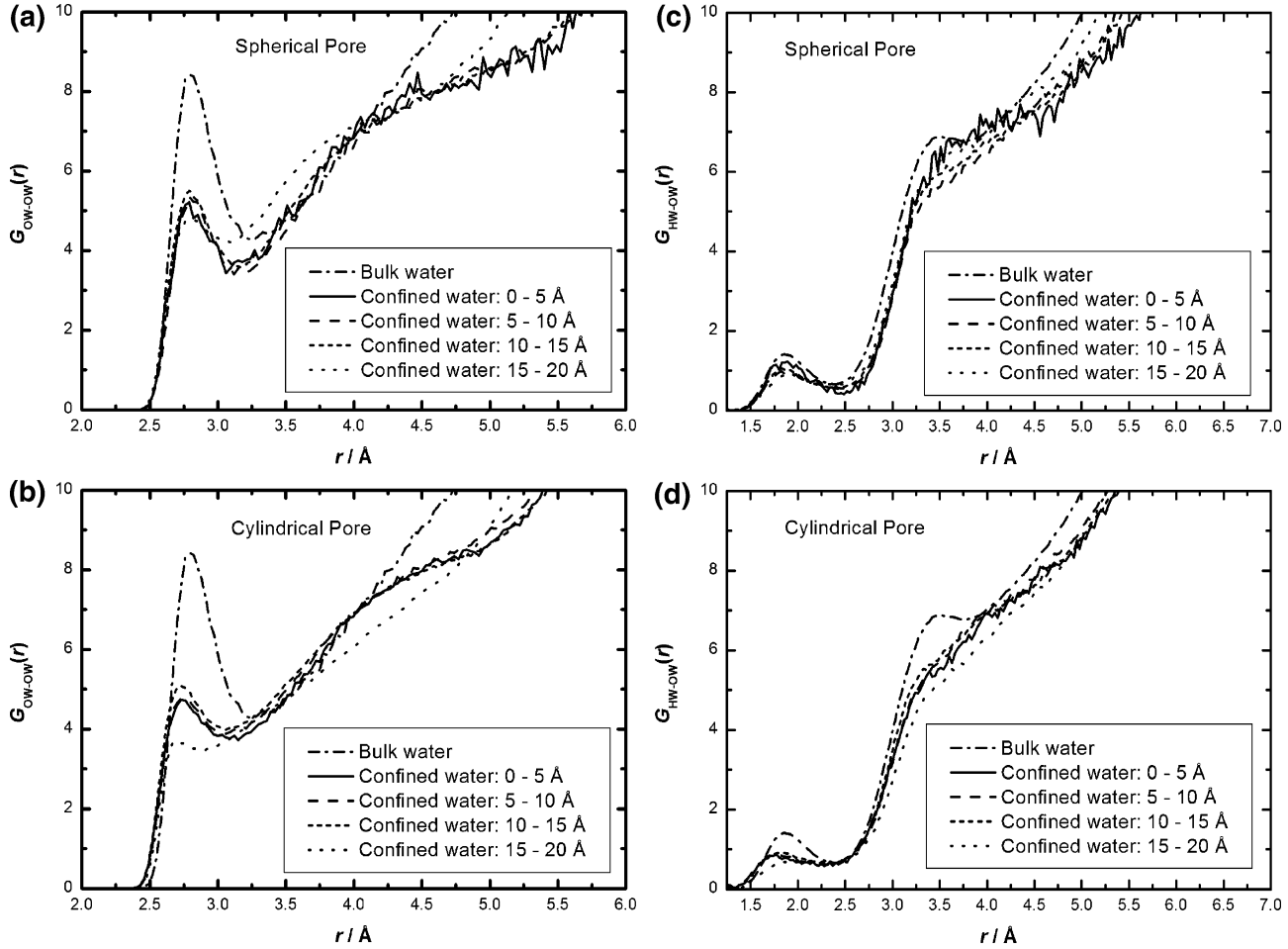

Figure 9. The radial distribution functions for (a) OW−all-O, spherical pore; (b) OW−all-O, cylindrical pore; (c) HW−all-O, spherical pore; and (d) HW−all-O, cylindrical pore, at varying distances from the pore center: 0−5, 5−10, 10−15, and 15−20 Å. The perturbation to the intermolecular structure of water is seen to extend from the vycor surface to the pore center.

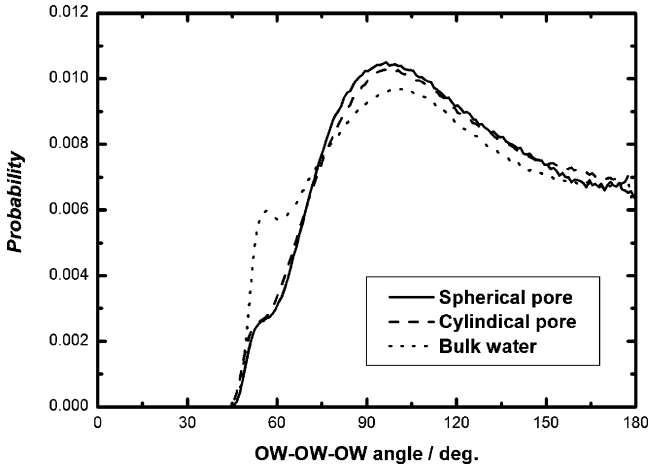

Figure 10. The OW−OW−OW angle distribution in confined water (spherical and cylindrical pore) and bulk water, calculated for OW−OW distances between 2.0 and 3.3 Å.

in the subsequent step is then set to the current potential plus the small perturbation. This procedure is run iteratively, until the difference between the fit and the data becomes insignificantly small such that there is no observable change in the empirical potential, or the modulus of the empirical potential energy reaches a preset limit.

The resulting configuration arising from the EPSR simulation therefore provides a 3-D model of the system which is consistent with the measured data, from which a complete set of atom−atom partial pair correlation functions can be extracted. In addition, the EPSR procedure allows the implementation of a spherical harmonic expansion[27] of the intermolecular structure in terms of polar coordinates r, θ and ϕ, in order to show the orientational correlations between molecules. A "spatial density plot" can be obtained by holding molecule 1 fixed at the origin in a pre-defined orientation and averaging over all possible positions and orientations of the second molecule within a minimum and maximum distance from the first molecule. This allows the directionality of the hydrogen bonding in the first shell to be investigated, and allows us to see the effect of confinement on the second hydration shell.

4. Results and Discussion

The EPSR fits to the dry vycor substrate and the confined water total structure factors are shown in Figure 7. Note that the data and fit have been scaled by factors of (number of vycor atoms/total number of atoms) and (number of water atoms/total number of atoms) respectively, as explained in section 3.3. Application of the empirical potential increased the goodness of fit to the data. It can be seen that small oscillations remain in the EPSR fits at low Q values, up to $\sim$1 Å^{-1}: these are essentially an artifact of the Fourier transform to Q-space. First, the length scale of the vycor pore (40 Å) is much larger than that of the water correlations (1−2 Å), and the low-Q data which would account for this are inaccessible due to the limits of the diffractometer.[10] Second, the size of the simulation cell is limited by computer power, and so only a single pore has been modeled

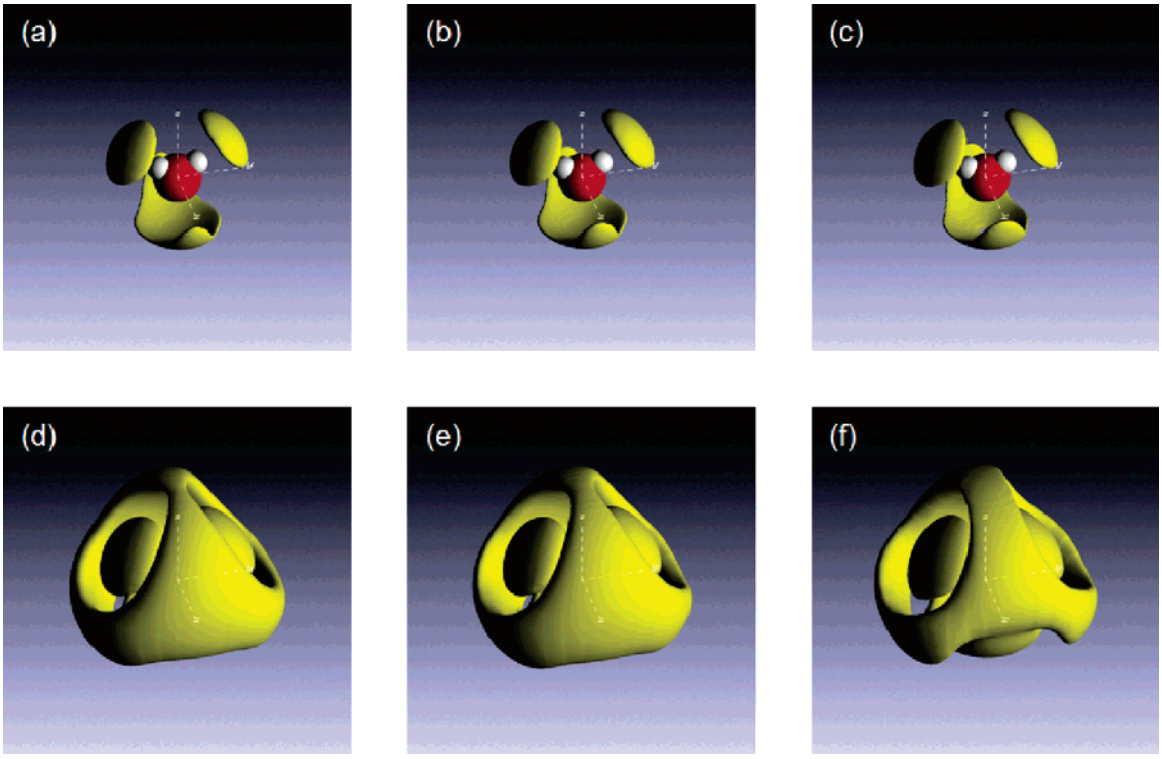

Figure 11. Spatial density functions for OW−OW correlations, $r = 2.2-5.5$ C. (a−c) fractional isosurface = 0.1; spherical pore, cylindrical pore, and bulk water respectively. (d−f) fractional isosurface = 0.4; spherical pore, cylindrical pore, and bulk water respectively.

in each instance. The consequences of this are that the $g(r)$s have not necessarily reached unity by half the box size (the cutoff for the Fourier transform to Q-space), and this manifests itself as oscillations in Q-space. A window function of $\cos(\pi r/2R_{max})$ has been applied in real space to minimize these artefacts.

Figure 8 shows the partial pair correlation functions for water confined in both a spherical and a cylindrical pore, and bulk water. In all three partials for OW−OW, OW−HW and HW−HW, it can be seen that the real-space distributions for the cylindrical and spherical pores are similar, despite the differences in the uniform atom distribution corrections noted in section 3.2, while the fits to the water total structure factors are indistinguishable. This indicates that the exact pore geometry used to model the vycor substrate is not critical in terms of the intermolecular water structure. The apparent differences between the water−water radial distribution functions for the spherical pore and cylindrical pore are much less pronounced than the difference between the functions for confined water and bulk water, as we shall see. However, in the case of the cylindrical pore, we see a slight inward shift of the first peak position as compared to the spherical pore, from 2.75 to 2.70 Å in the OW−OW partial, 1.78 to 1.72 Å in the OW−HW partial, and 2.36 to 2.26 Å in the HW−HW partial.

The use of the uniform atom distributions throughout the simulation means that it is possible to compare these partial pair correlation functions directly with those of bulk water. Significant differences are apparent. The first shell in the OW−OW distribution is much less sharp than for bulk water, and the coordination number is reduced from 4.3 ± 0.4 to 2.6 ± 0.4 (integrated to the first minimum). It is also possible to plot the OW−all-O radial distribution functions for water oxygen atoms at varying distances from the pore center. Panels a and b of Figure 9 show this OW−O distribution for the spherical pore and cylindrical pore, respectively, at distances from the pore center of 0−5 Å, 5−10 Å, 10−15 Å and 15−20 Å, and they show that the reduction in coordination number in the first shell extends to the center of the pore. This coincides with a contraction of the second hydration shell, from 4.5 Å in bulk water, to 3.9 Å in confined water.

In the case of the OW−HW and HW−HW functions, we still observe a significant change in the first hydrogen-bond peak, which decreases in amplitude and moves inward (from 1.81 to ∼1.77 Å in the OW−HW function) when the water is confined. Again, plotting the radial distribution function from water hydrogen atoms at varying distances from the pore center to all oxygen atoms (Figure 9c,d) show that the hydrogen-bonding disruption extends to the pore center (0−5 Å region). In the case of the spherical pore, the size of the first hydrogen-bonded peak increases slightly as the pore center is approached, but it never recovers the value found in bulk water. In addition, we observe a small increase in amplitude in the OW−HW partial pair correlation function at around 4 Å, similar to that observed in the experimentally derived $g_{XH}(r)$ in ref 5. Integration of the first OW−HW shell gives the number of hydrogen bonds per water molecule to be ∼2.2, in comparison to ∼3.6 in bulk water. These changes to the hydrogen-bonded structure of the water upon confinement are not merely artefacts arising from excluded volume effects, as these have been fully accounted for in the simulation. They represent a significant change in water's intermolecular structure. This is illustrated further in the OW−OW−OW angle distribution (Figure 10), calculated for all OW−OW distances between 2.0−3.3 Å (first shell). Upon confinement, a large decrease in the number of triangular water conformations (near 60°) is accompanied by a shift of the peak at ∼101° in bulk water to the smaller value of ∼96° upon confinement. This is in accord with the shift to lower r of the second peak in the OW−OW partial pair correlation function as seen in Figure 8. The reduced triangular conformation is consistent with the reduced density of confined water compared to the bulk, and suggests a more open structure upon confinement. On the other hand, the inward movement of the second OW−OW peak (Figure 8) and the corresponding change to the

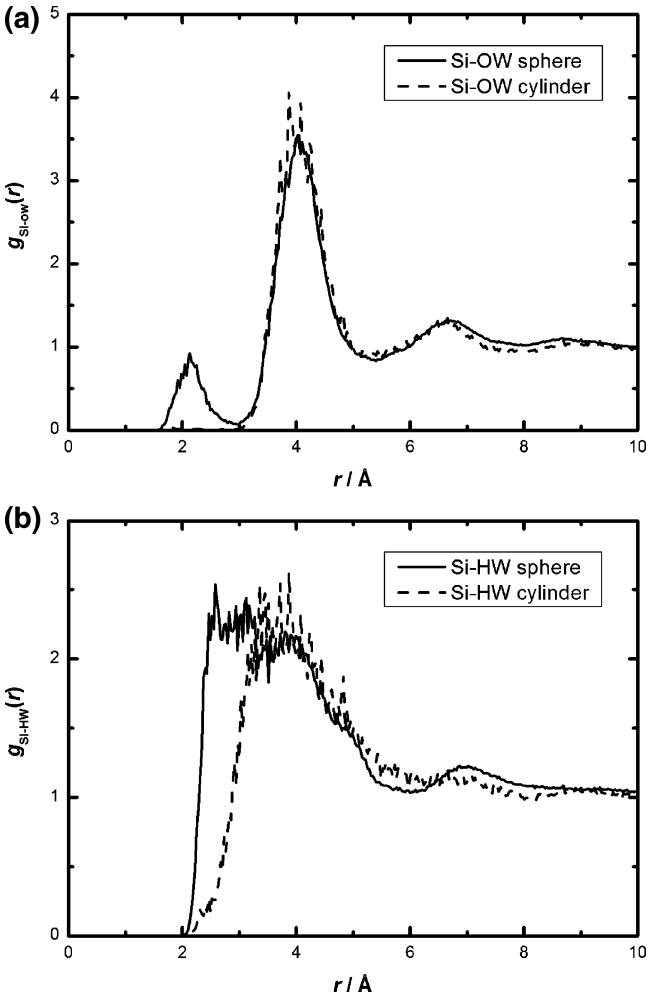

Figure 12. The substrate−water partial pair correlation functions: Si−OW and Si−HW, showing layering of the water in the pore. Note that the prepeak at 2.0 − is absent in cylinder.

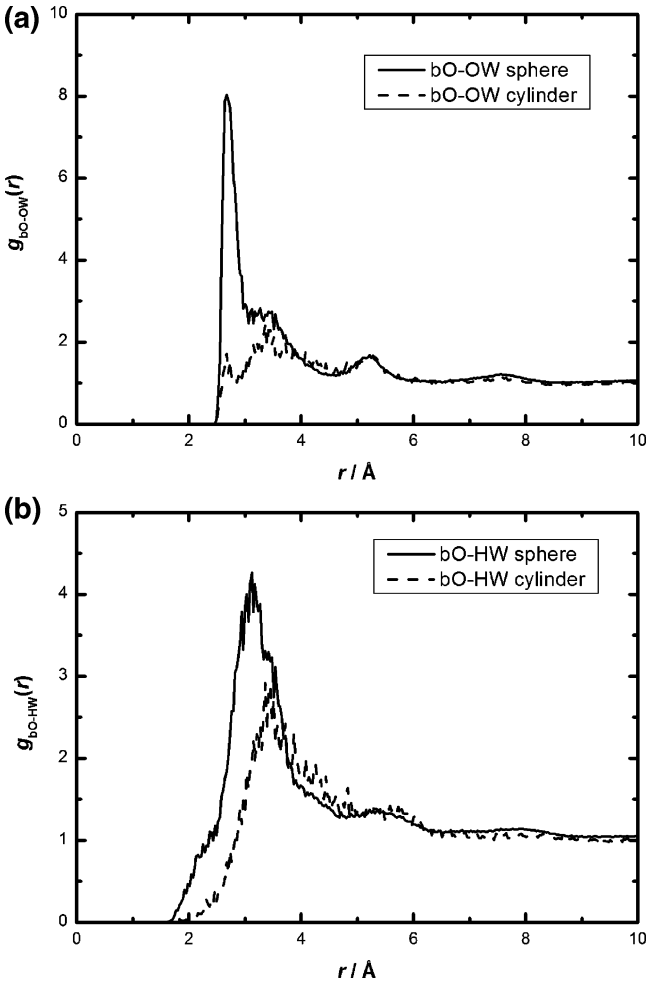

Figure 13. The substrate−water partial pair correlation functions: bO−OW and bO−HW, showing the layering of the water in the pore.

OW−OW−OW angle distribution (Figure 10) are reminiscent of what is seen in bulk water under pressure.[28,29]

From the spatial density plots shown in Figure 11, which show the most probable angular positions of the nearest neighbor water molecules, it appears that the first hydrogen-bonded shell does not change appreciably upon confinement, while the second shell shrinks marginally inward and becomes more contiguous with the first shell. Note that these relatively small changes compared to bulk water occur despite the sharp reduction in number of hydrogen bonds upon confinement, as observed above. We conclude that a reduction in the number of hydrogen bonds per water molecule does not necessarily imply strongly reduced tetrahedrality. The small change toward the bottom of the second-shell lobe upon confinement probably reflects the increased probability of OW−OW−OW correlations at higher angles (Figure 10). The marked changes in water's radial distribution functions observed here must therefore be a result of its confinement within a hydrophilic pore, but they do not apparently translate to a very marked change in its underlying three-dimensional structure.

Let us turn now to the nature of the vycor−water correlations, which are shown in Figures 12−15. The water−substrate interactions for both the spherical and cylindrical pores give rise to structure around the pore surface. The mean Si−OW distance is ∼4.1 Å, and in the case of the spherical pore, it appears that a small number of water molecules have percolated into the vycor substrate surface, giving a peak at a much smaller distance of ∼2.0 Å. The Si−HW correlations (Figure 12) have a peak around 4 Å, which may also be responsible for the increased amplitude around 4 Å in the $g_{XH}(r)$ function in ref 1. which includes substrate−water hydrogen correlations. The nearest-neighbor bO−OW distance is ∼2.7 Å, with the bO−HW distances being 3.1 and 3.4 Å for the spherical pore and cylindrical pore respectively. Large differences are indeed observed in the water−vycor partial pair correlation functions from the spherical pore and the cylindrical pore, and we suggest that these are perhaps due to the different curvatures of the pore surfaces in each case.

The correlations involving the pore surface atoms, nbO and H (Figures 14 and 15) are less reliable, probably due to the difficulty in calculating a realistic uniform atom distribution from annuli of only 1.5 Å thickness. This has given rise to much larger differences between the partial pair correlation functions calculated for the spherical pore and the cylindrical pore. Despite the differences in the geometries, we see clearly a hydrogen-bond peak between the saturating surface hydrogens and the water oxygens at ∼1.7 Å. The distance between the nonbridging oxygens and the water hydrogen atoms, however, is smaller than that between the nonbridging oxygens and the water oxygens. This means that the water molecule is orientated slightly, such that one water hydrogen atom is more toward the vycor substrate: the water is not orientated with the dipole moment directed away from the vycor surface OH group as one might expect. In turn, this leaves only one hydrogen atom available for forming hydrogen bonds with the surrounding water molecules. We therefore suggest that this hydrogen

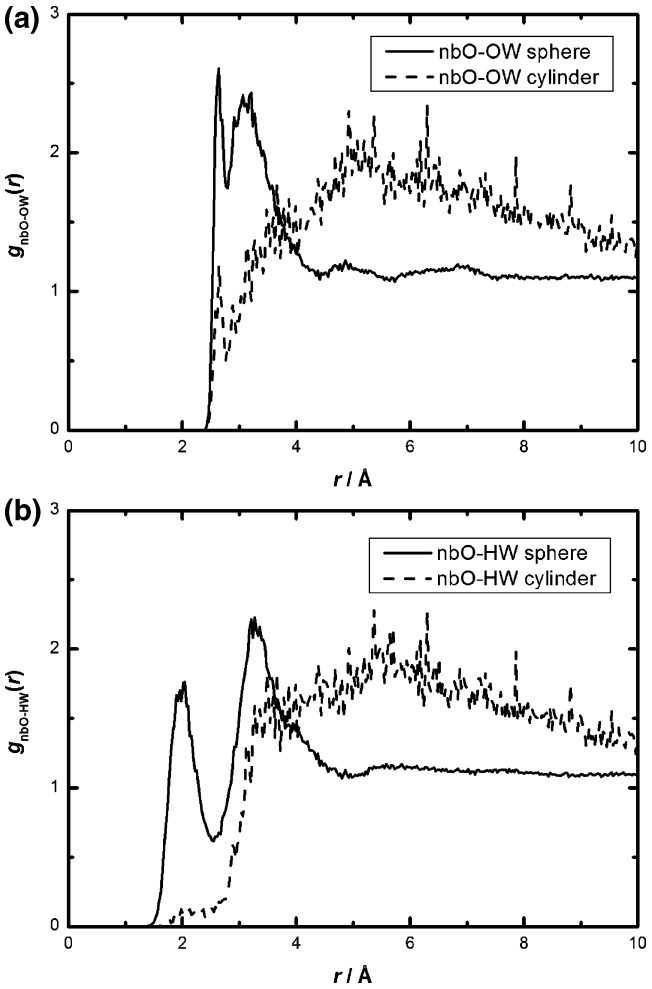

Figure 14. The substrate−water partial pair correlation functions: nbO−OW and nbO−HW, showing the interactions with the pore surface.

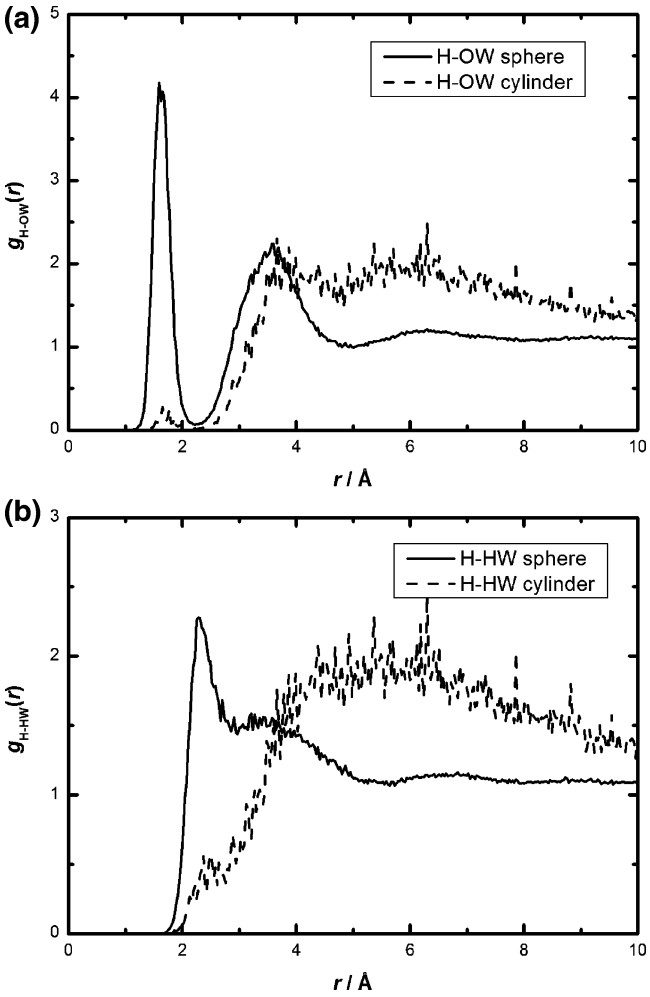

Figure 15. The substrate−water partial pair correlation functions: H−OW and H−HW, showing the interactions between the water and the hydrophilic O−H groups on the pore surface.

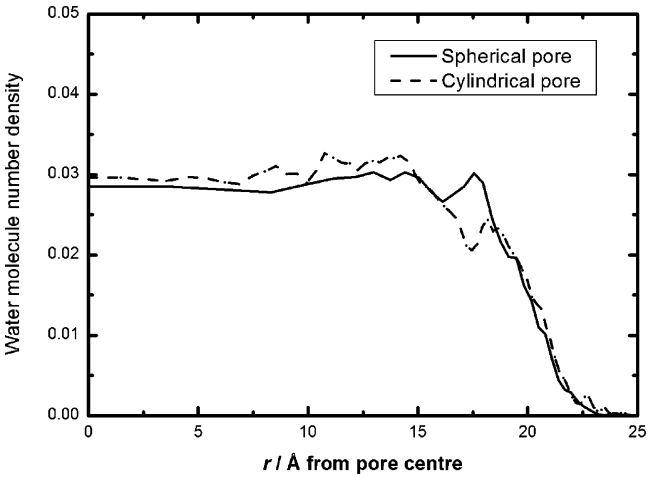

Figure 16. The water molecule density distribution across the pore: comparison between the spherical and cylindrical pores.

bonding of the nearest layer of water molecules with the substrate has a significant effect on the next layer of water molecules in terms of disrupting the water−water hydrogen bonding. The fact that the radial distribution functions for OW−O and HW−O are similar for water molecules at different distances from the vycor surface also leads us to believe that these orientations adopted near the surface carry through to water molecules nearer the pore center. Via this mechanism, the usual 4-fold coordination of water in the bulk is broken upon confinement, giving rise to only half the number of hydrogen bonds per molecule, even at the pore center. This process of breaking of hydrogen bonds in confined water would no doubt raise the entropy of the liquid compared to the bulk, thus allowing significant supercooling of the water to take place, as does indeed happen.[30] Previous simulation work which considers the variation of the hydrogen-bond network as one moves across the pore[31,32] also results in a large decrease in the number of water−water hydrogen bonds near the vycor surface, and indeed toward the center of the pore, the number of hydrogen bonds per molecule at a high hydration level is still lower than the number of bonds formed in bulk SPC/E water.

Figure 16 shows the density distribution of water across the pore, calculated as a function of the distance from the center of the pore (using *x*, *y*, and *z* atomic co-ordinates in the case of the spherical pore, or using just *x* and *y* co-ordinates when calculated for the cylindrical pore). The density distributions have been calculated such that the *r*-values of the histogram give the same volume integral in each case, i.e, the *r*-values are more widely spaced nearer the center of the pore, to avoid the counting statistics becoming worse toward the center of the pore. The feature which both distributions have in common is the decreased density near the pore surface, and then a peak in the density at around 17.6 or 18.2 Å for the spherical and cylindrical pore respectively. These findings are in close agreement with molecular dynamics simulations performed on this system.[12,31−33]

5. Conclusions

In this paper we have demonstrated the need for a full atomic-level analysis of confined fluid systems, which is consistent with the available diffraction data, and makes no a-priori assumptions about the water or vycor structure. We have shown that the contributions to structure factors from the confined fluid also include a significant contribution from cross−terms (substrate−confined fluid correlations) which cannot be considered negligible: hence simulations or experiments which do not take this into account are unable to present the complete picture of the intermolecular structure of confined fluids and their interaction with the pore surface. The problems encountered in coming to a full understanding of how to incorporate diffraction data into a complex simulation of a confined fluid have been outlined: including calculations of the uniform atom distributions necessary to be able to compare the results directly with those of bulk water.

The method described has been demonstrated on the system of water confined in vycor. Two different pore geometries were chosen for the analysis, and it has been shown that the actual pore shape has little or no effect on the intermolecular structure of confined water, although differences are apparent in the water−substrate pair correlation functions and the density distribution of water across the pore. Comparison with bulk water, however, has shown that there is an appreciable decrease in the hydrogen-bonding upon confinement: the number of hydrogen bonds per water molecule is only ∼2.2 in confined water, as compared to ∼3.6 in bulk water. In addition, there is a decrease in the number of water molecules in the first hydration shell, and the second shell moves inward by ∼0.6 Å. This perturbation in water's intermolecular structure is found to extend from the region near the vycor surface into the center of the pore.

The analysis has also investigated the nature of the substrate−water interactions; showing that there is in fact structure arising from interactions between the water and the pore wall. We observe that water interacts strongly with the pore surface and explains the slowing-down of molecular motions compared to the bulk. The density distribution varies across the pore, with a lower density than average near the vycor surface, followed by a peak in the density at ∼2 Å from the pore wall. The vycor substrate−water correlations show evidence of hydrogen bonding between the first layer of water molecules and the OH groups on the vycor surface. Given that the water intermolecular radial distribution functions are very similar even at varying distances from the vycor surface, we suggest that the water structure throughout the pore is imposed by the first surface layer, where hydrogen bonding to the vycor OH groups causes a marked reorientation of the water molecules near the surface, leaving only one hydrogen atom per water molecule available to donate a hydrogen bond to the next layer of water molecules. In turn, this disrupts the hydrogen bond network between water molecules further from the surface, and is a significant factor in the mechanism behind the observed supercooling of water in confinement.

Acknowledgment. The experimental data have been collected within the Agreement No.01/9001 between CCLRC and CNR, concerning collaboration in scientific research at the spallation neutron source ISIS and with partial financial support of CNR.

References and Notes

(1) Dore, J. C. Chemical Physics. *Chem. Phys.* **2000**, *258*, 327.

(2) Bellissent-Funel, M.-C. *J. Phys. Condensed Matter* **2001**, *13*, 9165.

(3) Gelb, L. D.; Gubbins, K. E.; Radhakrishnan, R.; Sliwinska-Bartkowiak, M. *Rep. Prog. Phys.* **1999**, *62*, 1573−1659.

(4) Teixeira, J.; Zanotti, J. M.; Bellissent-Funel, M.-C.; Chen, S. H. *Physica B* **1997**, *234*−*236*, 370−374.

(5) Bruni, F.; Ricci, M. A.; Soper, A. K. *J. Chem. Phys.* **1998**, *109* (4), 1478.

(6) Webber, B.; Dore, J. *J. Phys.: Condens. Matter* **2004**, *16*, S5449−S5470.

(7) Steytler, D. C.; Dore, J. C. *Mol. Phys.* **1985**, *56*, 1001.

(8) Steytler, D. C.; Dore, J. C.; Wright, C. J. *Mol. Phys.* **1983**, *48*, 1031.

(9) Bellissent-Funel, M.-C.; Sridi-Dorbez, R.; Bosio, L. *J. Chem. Phys.* **1996**, *104* (24), 10023−10029.

(10) Soper, A. K.; Bruni, F.; Ricci, M. A. *J. Chem. Phys.* **1998**, *109* (4), 1486.

(11) Puibasset, J.; Pellenq, R. J. *J. Phys.: Condens. Matter* **2004**, *16*, S5329.

(12) Rovere, M.; Gallo, P. *J. Phys.: Condens. Matter* **2003**, *15*, S145−S150.

(13) Ricci, M. A.; Bruni, F.; Gallo, P.; Rovere, M.; Soper, A. K. *J. Phys.: Condens. Matter* **2000**, *12*, A345−A350.

(14) Tombari, E.; Salvetti, G.; Ferrari, C.; Johari, G. P. *J Chem. Phys.* **2005**, *122*, 104712.

(15) Bellissent-Funel, M.-C.; Chen, S. H.; Zanotti, J. M. *Phys. Rev. E* **1995**, *51*, 4558.

(16) Gallo, P.; Rovere, M.; Spohr, E. *Phys. Rev. Lett.* **2000**, *85*, 4317.

(17) Liu, L.; Faraone, A.; Mou, C. Y.; Yen, C. W.; Chen, S. H. *J. Phys.: Condens. Matter* **2004**, *16*, S5403.

(18) Hiejima, Y.; Yao, M. *J. Phys.: Condens. Matter* **2004**, *16*, 7903.

(19) Soper, A. K. *Chem. Phys* **1996**, *202*, 295.

(20) Soper, A. K. *Mol. Phys* **2001**, *99*, 1503.

(21) Bowron, D. T.; Finney, J. L.; Soper, A. K. *J. Phys. Chem. B* **1998**, *102*, 3551.

(22) Soper, A. K.; Howells, W. S.; Hannon, A. C. *ATLAS - Analysis of Time-of-flight diffraction data from Liquid and Amorphous Samples*; Report RAL-89-046; Rutherford Appleton Laboratory: 1989.

(23) Soper, A. K.; Luzar, A. *J. Chem. Phys.* **1992**, *97* (2), 1320.

(24) Berendsen, H. J. C.; Grigera, J. R.; Straatsma, T. P. *J. Phys. Chem.* **1987**, *91*, 6269.

(25) Soper, A. K. *J. Phys.: Condens. Matter* **1997**, *9*, 2399.

(26) Soper, A. K. *Phys. Rev. B* **2005**, *72*, 104204.

(27) Bowron, D. T.; Soper, A. K.; Finney, J. L. *J. Chem. Phys.* **2001**, *114* (14), 6203.

(28) Okhulkov, A. V.; Damianets, Y. N.; Gorbaty, Y. E. *J. Chem. Phys.* **1994**, *108*, 9859.

(29) Soper, A. K.; Ricci, M. A. *Phys. Rev. Lett.* **2000**, *84* (13), 2881−2884.

(30) Bellisent-Funel, M.-C.; Lal, J. C.; Bosio, L. *J. Chem. Phys.* **1993**, *98*, 4246−4252.

(31) Spohr, E.; Hartnig, C.; Gallo, P.; Rovere, M. *J. Mol. Liq.* **1999**, *80*, 165−178.

(32) Hartnig, C.; Witschel, W.; Spohr, E.; Gallo, P.; Ricci, M. A.; Rovere, M. *J. Mol. Liq.* **2000**, *85*, 127−137.

(33) Gallo, P.; Ricci, M. A.; Rovere, M. *J. Chem. Phys.* **2002**, *116* (1), 342−346.